Directional results and absolute archaeointensity determination by the classical Thellier and the multi-specimen DSC protocols for two kilns excavated at Osterietta, Italy

Directional results and absolute archaeointensity determination by the classical Thellier and the multi-specimen DSC protocols for two kilns excavated at Osterietta, Italy

EVDOKIA TEMA[1], PIERRE CAMPS[2], ENZO FERRARA[3] AND THIERRY POIDRAS[2]

1 Dipartimento di Scienze della Terra, Università degli Studi di Torino, via Valperga 35, I-10125 Torino, Italy (evdokia.tema@unito.it)

2 Géosciences Montpellier, CNRS and Université Montpellier 2, Montpellier, France

3 Istituto Nazionale di Ricerca Metrologica, Strada delle Cacce 91, I-10135 Torino, Italy

Received: January 30, 2015; Revised: April 7, 2015; Accepted: April 11, 2015

ABSTRACT

We present a detailed rock-magnetic and archaeomagnetic study of two brick kilns, named OSA and OSB, discovered at the location of Osterietta, in northern Italy. The magnetic properties of representative samples have been investigated to identify the nature of the magnetic carriers, their domain state and thermal stability, and investigate their suitability for archaeomagnetic determinations. Thermally stable, mainly pseudo-single domain (PSD) magnetite is identified as the main magnetic carrier. The full geomagnetic field vector has been determined for the two kilns, including directional and intensity analysis. Archaeointensities have been recovered with both the classical Thellier and the multi-specimen protocols. The multi-specimen procedure was performed with a very fast-heating oven developed at Montpellier, France. A Matlab® code for anisotropy correction during the Thellier experiment is provided. The archaeointensity results obtained from both techniques for the OSA kiln are of high quality and in good mutual agreement. For the OSB kiln, Thellier results are characterized by large standard deviation and the multi-specimen (MSP) technique was not successful. The obtained full geomagnetic field vector (declination, inclination and intensity) has been used for the archaeomagnetic dating of the two structures suggesting that the OSA kiln was for the last time used between 1761–1841 A.D. and the OSB kiln between 1752–1831 A.D., at 95% probability. This study shows that intensity determinations do not restrict the dating results when referring to the last few centuries, as this period is characterized by very small intensity variations.

Keywords: secular variation, geomagnetic field vector, archaeomagnetic dating, Italy

Stud. Geophys. Geod., 59 (2015), 554–577, DOI: 10.1007/s11200-015-0413-0

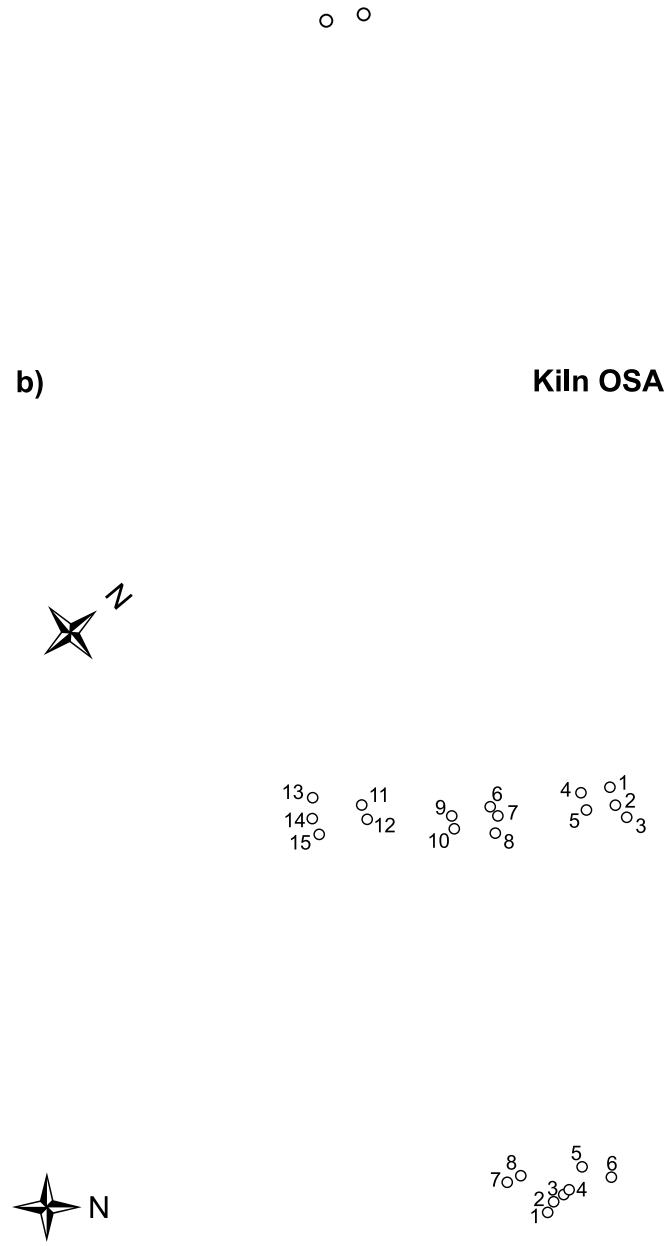

Fig. 2. **a)** General view of the position of the OSA and OSB kilns, situated near the city of Alessandria and its old cittadella. **b)** and **c)** Photos and positions of the samples collected from kilns OSA and OSB, respectively.

(*Venturino et al., 2013*). However, the very limited amount of material sampled at the initial phase of the excavation (July 2010) for TL analysis has not allowed a complete and detailed TL investigation (*Raimondo Prosperi, ARKAIA, personal communication*). Furthermore, the proposed TL date has been calculated only from the total absorbed TL dose without including measurements of the environmental and annual dose, and the corresponding corrections. The available TL date can thus be used only as a general reference and does not offer a precise dating.

For archaeomagnetic analysis, a total of 15 brick hand samples from the OSA kiln have been collected (Fig. 2b), coming from the three first tunnels (numbered 1 to 6 from East to West). From the OSB kiln, 8 brick hand samples have been collected from the preafurnia tunnels (Fig. 2c). All collected samples were oriented *in situ* with a magnetic compass and an inclinometer, signing the orientation arrow directly on the bricks' surface. No consolidation at the laboratory was needed as the bricks were very compact and well conserved. Bad weather conditions prevented the use of a sun compass. From each independently oriented brick, at least four cylindrical specimens of standard dimensions (diameter = 25.4 mm, height = 22 mm) were drilled in the laboratory. The prepared specimens were used for magnetic mineralogy experiments and for the determination of the archaeomagnetic direction and intensity.

3. MAGNETIC MINERALOGY

The magnetic properties of the collected bricks have been investigated to identify the nature of the magnetic carriers, their domain state behaviour and their thermal stability with the objective to check their suitability for archaeomagnetic determinations. Isothermal remanent magnetization (IRM) acquisition curves, thermal demagnetization of three-axes IRM components (*Lowrie, 1990*), hysteresis loops and low-field thermomagnetic curves were measured for pilot samples.

IRM acquisition curves of representative samples were obtained at the ALP Palaeomagnetic laboratory (Peveragno, Italy) with an ASC pulse magnetizer to impart the IRM, applying stepwise increasing magnetic fields up to 1.6 T, and a JR6 spinner magnetometer (AGICO) to measure the remanent magnetization. The obtained curves for both OSA and OSB kilns are very similar, with a saturation of the magnetization reached at low fields varying from 0.2 to 0.4 T (Fig. 3). This observation is consistent with the presence of a low-coercivity mineral such as magnetite. Such interpretation is further supported by the thermal demagnetization experiments of a three component IRM (*Lowrie, 1990*). A composite orthogonally induced IRM was imparted to representative samples: first a maximum field (1.6 T) was applied along the cylinder axis (*Z*), then an intermediate field (0.5 T) along the *Y* axis and finally a minimum field (0.1 T) along the *X* axis. Stepwise thermal demagnetization results of the three-axes IRM (Fig. 4) show the dominance of the magnetically soft fraction (< 0.1 T); however, in some samples mainly from the OSB kiln (Fig. 4c,d) the medium coercivity component is also important while the high coercivity component is in all cases negligible.

Hysteresis measurements were performed with a Lake Shore 7400 Vibrating Sample Magnetometer (VSM) equipped with a chamber for low temperature (liquid nitrogen) measurement at INRIM (Torino, Italy). Five samples from the OSA kiln have been

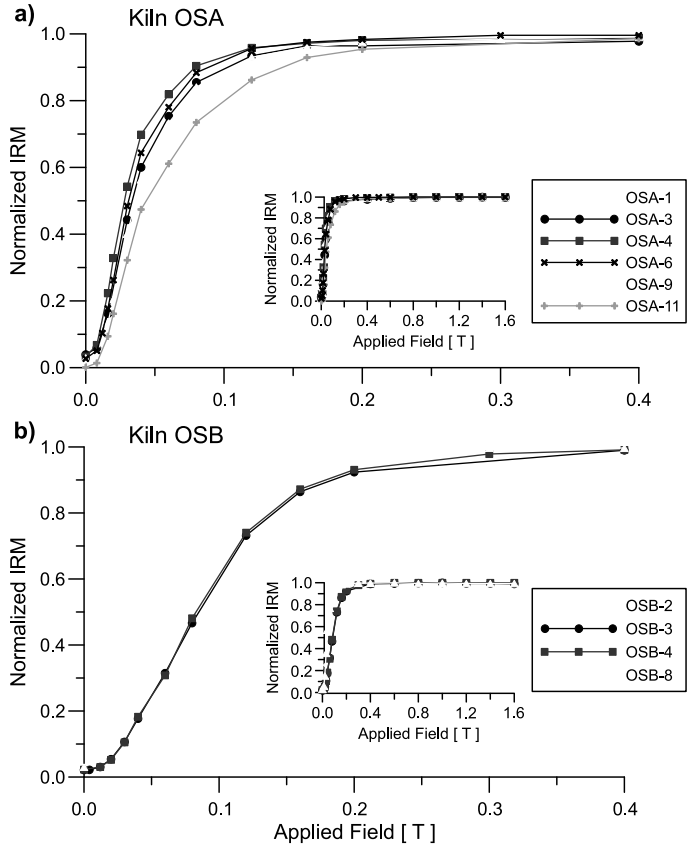

Fig. 3. Normalized isothermal remanent magnetization (IRM) acquisition curves up to 0.4 T for representative samples from **a)** kiln OSA and **b)** kiln OSB. Insets show the same IRM curves up to 1.6 T.

analysed. The hysteresis curves obtained at room temperature for representative samples (OSA-3, OSA-16 and OSA-19) show the coexistence of different magnetic contributions (Fig. 5a). The analysed powders exhibit, in fact, a ferrimagnetic behaviour along with paramagnetic contributions. For further investigation of the ferrimagnetic carriers, hysteresis loops have been corrected for the paramagnetic contribution (Fig. 5a–c). The shape of the loops and the low value of the coercive field suggest the presence of a soft magnetic phase, such as magnetite. Fig. 5b,c shows the changes with temperature of the magnetization cycles exhibited by samples OSA-4 and OSA-7, respectively, in the temperature range from –196°C to 25°C. From the graphs, a significant content of ferromagnetic pseudo-single domain particles can be appreciated, which is related to the hysteretic behaviour and maintained at all the applied temperatures. The change of the shape of the hysteresis curves with temperature observed in Fig. 5b,c is probably due to the presence of smaller particles that progressively unblock their magnetization moving

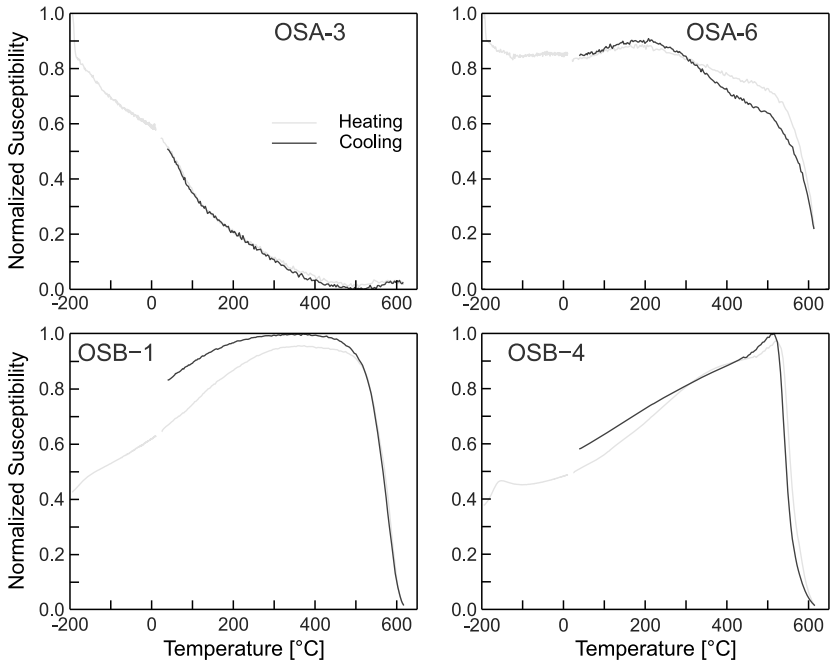

Fig. 6. Dependence of weak-field susceptibility on temperature for representative samples from kilns OSA and OSB.

4. ARCHAEOMAGNETIC FIELD VECTOR DETERMINATION

4.1. Archaeomagnetic direction

One specimen per sample from the OSA and OSB kilns has been selected for the determination of the archaeomagnetic direction of each kiln. First, the natural remanent magnetization (*NRM*) of 15 specimens from OSA and 8 specimens from OSB was measured at the ALP Palaeomagnetic laboratory with a JR-6 spinner magnetometer. Following, all specimens have been stepwise thermally demagnetized from room temperature up to 580°C with a Schonstedt TSD-2 furnace. The demagnetization results are illustrated as orthogonal vector projections of the remanent magnetization (*Zijderveld, 1967*) (Fig. 7). Zijderveld diagrams show that the magnetic remanence is very stable and it consists of one well defined characteristic remanent magnetization (*ChRM*) direction.

The directions of the *ChRM* for each specimen were evaluated from principal component analysis (*Kirschvink, 1980*). Directions calculated at specimen level are well defined with maximum angular deviation (*MAD*) generally lower than 2°. Four specimens from OSA kiln were rejected as their corresponding Zijderveld diagrams didn't pass through the origin of the axes. Results from both OSA and OSB kilns at specimen level are reported in Table 1, together with the mean direction for each kiln. The statistical parameters are calculated assuming a Fisherian distribution (*Fisher, 1953*). Equal-area

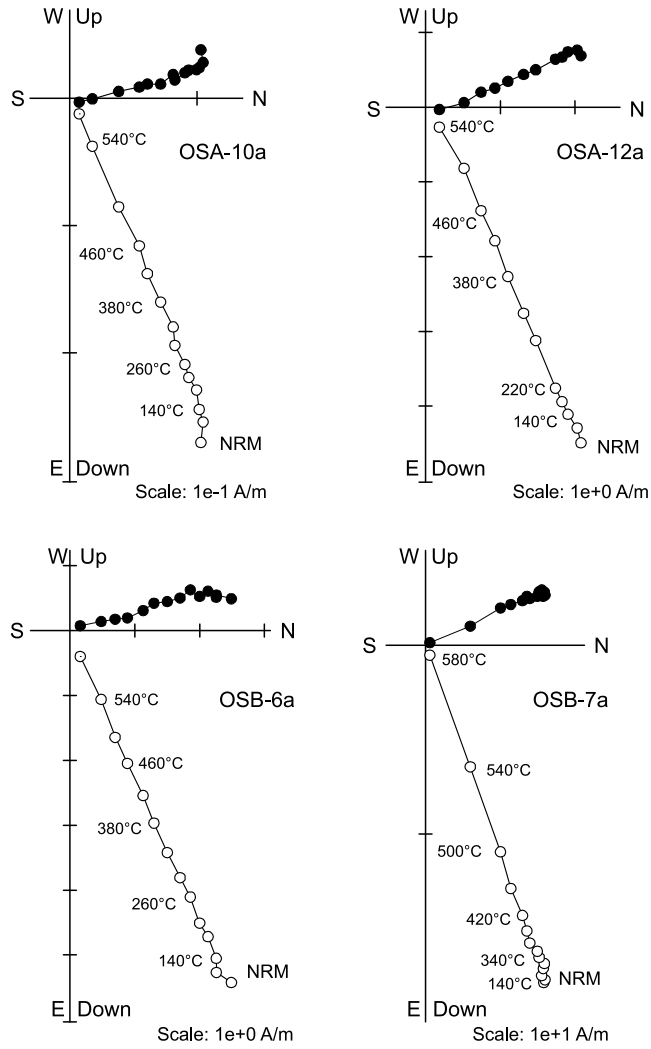

Fig. 7. Stepwise thermal demagnetization results from representative samples from kilns OSA (upper part) and OSB (lower part) illustrated as Zijderveld plots. Symbols: full dots: declination; open dots: apparent inclination.

projections of the *ChRM* directions (Fig. 8) show a very good concentration around the mean values. The calculated mean direction for kiln OSA is: declination $D = 341.8°$, inclination $I = 66.2°$, precision parameter $k = 389$, confidence angle $\alpha_{95} = 2.3°$ and for kiln OSB is: $D = 339.6°$, $I = 67.5°$, $k = 504$, $\alpha_{95} = 2.5^{o}$.

Table 1. Archaeomagnetic directional results. *D*: declination; *I*: inclination; *MAD*: maximum angular deviation; Mean value: *N*: number of independently oriented samples; D_m: mean declination; I_m: mean inclination; *k*: precision parameter; α_{95}: 95% semi-angle of confidence according to *Fisher (1953)*.

Sample	Temperature Interval [°C]	*D* [°]	*I* [°]	*MAD* [°]
Kiln OSA:				
OSA-1a	180–580	334.5	64.2	1.5
OSA-2a	180–580	354.0	68.5	1.3
OSA-3a	220–580	335.4	68.4	0.9
OSA-4a	140–580	354.9	68.5	1.3
OSA-5a	140–540	354.2	67.3	1.7
OSA-6a	220–580	341.7	63.8	1.2
OSA-7a	100–580	329.6	64.1	2.1
OSA-9a	260–580	334.3	64.2	1.1
OSA-10a	140–580	345.5	66.5	1.7
OSA-12a	140–580	336.9	64.2	1.6
OSA-14a	260–580	344.3	65.8	1.5
Mean values:				
$N = 11$	$D_m = 341.8°$	$I_m = 66.2°$	$k = 389$	$\alpha_{95} = 2.3°$
Kiln OSB:				
OSB-1a	100–580	329.3	69.7	1.8
OSB-2a	140–580	349.3	70.7	1.2
OSB-3a	180–580	340.8	70.8	1.3
OSB-4a	380–580	342.2	63.3	1.1
OSB-5a	180–580	339.2	66.4	1.2
OSB-6a	260–580	342.5	64.8	1.6
OSB-7a	140–580	335.7	68.5	1.3
OSB-8a	140–580	337.9	64.9	1.0
Mean values:				
$N = 8$	$D_m = 339.6°$	$I_m = 67.5°$	$k = 504$	$\alpha_{95} = 2.5°$

4.2. Archaeomagnetic intensity

Experimental procedure

Absolute intensity determinations were carried out with both the *Thellier and Thellier (1959)* in its classical form and the multi-specimen protocols (*Biggin and Poidras, 2006*; *Dekkers and Böhnel, 2006*; *Fabian and Leonhardt, 2010*). This double approach was possible as material was available in sufficient quantity. The main motivation of a double approach was to provide an additional reliability check with a multi-method consistency. All archaeointensity measurements were carried out at the Palaeomagnetic laboratory of Géosciences Montpellier.

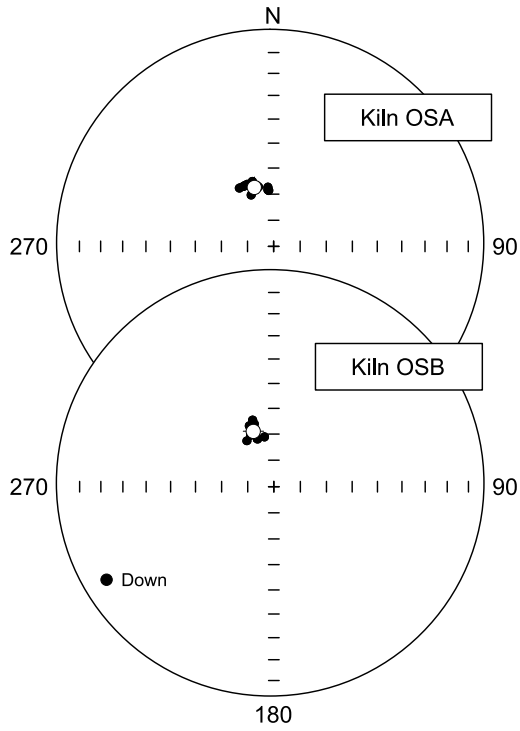

Fig. 8. Equal area projection of the characteristic remanent magnetization (*ChRM*) directions for kilns OSA and OSB. The big dot represents the mean value calculated for each kiln.

The classical Thellier protocol was applied on 56 samples; 32 from OSA kiln and 24 from OSB. On the basis of the rock magnetic investigations carried before the palaeointensity measurements, no *a priori* sample selection was performed. The ChRMs are clearly of thermoremanent origin, not disturbed by significant secondary components, and the magnetic properties seem to be reasonably stable during the laboratory heating. The measurement protocol is as follows. The samples are heated and cooled twice at each temperature step in presence of a 50 μT induction field during cooling. The field is oriented along the cylinder axis of the core (*Z* axis) for the first cycle and in the opposite direction for the second one. Samples were heated in 11 steps between 120°C and 560°C: steps of 60°C were applied between 120 and 300°C, 50°C between 300 and 400°C, 40°C between 400 and 480°C and finally 30°C between 480 and 540°C. After every two-temperature steps, a *pTRM* check was performed to detect any alteration in the thermoremanent magnetization acquisition capacity. All heating-cooling cycles were performed in air. In our palaeointensity furnace, the temperature reproducibility between heating treatments at the same step is within 1°C, and the intensity of laboratory field is maintained with a precision better than 0.1 μT (*Camps et al., 2011*). After each heating-cooling cycle, the remanent magnetization was measured with a 2G cryogenic magnetometer.

The Thellier archaeointensity measurements were corrected for magnetic anisotropy effect by means of the anisotropy of *TRM* (*ATRM*) according to a standard procedure adopted in the Montpellier laboratory (see *Fanjat et al., 2013*). The *ATRM* tensors were determined during the Thellier experiment, at a temperature step for which at least 20% of the initial *NRM* is involved for the majority of samples. In this study, a temperature of 440°C has been chosen. The samples were remagnetized at this temperature after the Thellier step (that yields $+Z$ and $-Z$ steps) in $+X$, $-X$, $+Y$, and $-Y$ directions. All archaeointensity values were corrected for the *ATRM* according to *Veitch et al. (1984)* method. Our Matlab® code estimating this correction is provided and illustrated with a data example as supplementary material. Just after the *ATRM* tensor determination at 440°C, the effect on the cooling rate on the acquisition of the *TRM* was estimated by repeating the last *pTRM* check with a 4-times slower cooling rate (12 h) than the one used in the Thellier protocol (3 h). The low cooling rate is simply achieved by switching off the fans of the cooling system of our furnace during the *pTRM* acquisition.

The multi-specimen (MSP) experiments were performed with a prototype of a very fast-heating infrared furnace developed in Montpellier (FURéMAG, patent #1256194). Two key points determine its characteristics. The first is to heat uniformly a single rock sample of a 10-cm^3 standard volume very fast. The second is to apply to the sample during the heating (and the cooling) a precise magnetic induction field, perfectly controlled in 3D with a measured precision better than 1° (*Camps et al., unpublished results*). The MSP-DSC protocol (*Fabian and Leonhardt, 2010*) was applied to both OSA and OSB kilns. As in this protocol the *pTRM* is imparted along the *NRM* direction, anisotropy correction is not necessary. During the test and the calibration of this furnace, *Fanjat (2012)* showed that it is also not necessary to apply cooling rate correction with the MSP protocol. The heating temperature for the multi-specimen experiments has been chosen with the criterion to be high enough to work on a sufficient fraction of the *TRM* (at least 20%) but sufficiently low to avoid chemical alteration. Based on the thermal demagnetization results obtained during the directional analysis, a temperature of 400°C has been chosen for all samples to impart the laboratory *pTRM*.

Archaeointensity results

The Thellier archaeointensity data were interpreted with the Thellier-tool software provided by *Leonhardt et al. (2004)*. We adopted a standard set of criteria derived from those proposed by *Fanjat et al. (2013)* and based on the statistical parameters introduced by *Coe et al. (1978)* and modified by *Prévot et al. (1985)* to interpret each individual archaeointensity data and filter out those of poor technical quality. Archaeointensity values at specimen level are accepted when the linear segment in the Arai plots is defined by more than four points ($n > 4$) and spans over 50% of the total extrapolated *ChRM*. We quantified the difference between two *pTRM* acquisitions at the same temperature by the difference ratio (*DRAT*) parameter (*Selkin and Tauxe, 2000*). *DRAT* is expressed in percent and corresponds to the maximum difference measured between repeated *pTRM* acquisition normalized by the length of the selected *NRM-TRM* segment. A maximum acceptable threshold is fixed arbitrarily at 10%, even though for most of our accepted results is lower than 5%. Jointly, we checked on the directional plots computed from the archaeointensity experiments that the *NRM* fraction used to calculate the archaeointensity

corresponds effectively to the *ChRM* direction of the core. For instance, the low-temperature part of the *NRM* may contain natural secondary magnetizations, and a spurious remanent magnetization acquired during the laboratory heating may superpose to the *NRM* if chemical changes in the magnetic minerals occurred. In total, 34 out of the 56 analyzed samples satisfied the quality criteria mentioned above and yielded acceptable archaeointensity determinations. The selected values at specimen level are listed in Table 2 and representative examples are illustrated in Fig. 9. Among the 22 excluded samples, 14 are rejected because of curvature in the Arai plots in spite of a good linearity in the Zijderveld plots, 5 are rejected because of a multi-component behavior observed in the Zijderveld plot, and 3 are rejected because of a too small *NRM* fraction destroyed ($f \leq 0.5$) before irreversible magneto-chemical changes arise. Note that in the cases where two slopes are present in the Arai's diagrams (see for example sample OSA-7c in Fig. 9), we have chosen the temperature interval that yields a palaeointensity value more similar to the other determinations.

Averaging the 23 acceptable results from kiln OSA, we found an archaeointensity value of 50.6 ± 2.2 μT. The individual values are fairly coherent as attested by the small value of the standard deviation (less than 5% of the average). A different case arises for kiln OSB for which a large scatter in the individual values is observed. Kiln OSB yields an archaeointensity value of 47.1 ± 6.9 μT, based on 11 acceptable results (Table 2). The large standard deviation, which is about 13% of the average, casts doubt on the reliability of this determination and it should be therefore cautiously used for archaeomagnetic dating.

The MSP archaeointensity results are processed in two steps. First, we selected "a posteriori" the samples for which the ratio between the fraction of *NRM* overprinted by the laboratory *pTRM* and the total *NRM* is between 0.2 and 0.8. This selection ensures that, if present, the multidomain *pTRM*-tail effect (see e.g. *Dunlop and Özdemir, 2000*) will be correctly measured. In addition, only samples for which the angle between the *NRM* and the *NRM* remaining after the laboratory *pTRM* overprint is lower than a threshold angle here arbitrarily chosen to be 10°, have been selected. This selection ensures that the *NRM* is the *ChRM*. Second, the MSP archaeointensities were determined by fitting the data with robust linear regression that is anchored to the point $(0, -1)$ for the fraction and domain state corrected values (see *Fabian and Leonhardt, 2010*, for a detailed explanation on this protocol and its treatment). The robust regression is used to minimize the influence of outliers by iteratively weighting the data by their distance to the fitting line (*Holland and Welsh, 1977*). We anchored the linear regression to the point $(0, -1)$ since it represents a theoretical reference: when a sample is cooled in zero field there is no *pTRM* acquisition. We estimated the effect of the value of alpha parameter for the domain state correction (*Fabian and Leonhardt, 2010*) by comparing the archaeointensities computed for a value of 0.5 with the two archaeointensities calculated by means of the two extreme values of 0.2 and 0.8.

MSP results are reported in Table 3 and illustrated in Fig. 10. For kiln OSA, from 10 samples measured, only 2 were rejected from the analysis because of a low *NRM* fraction for the first one and significant change in direction after *pTRM* acquisition for the second one. The eight samples selected yield a very similar palaeointensity value whatever the protocol used (DB, FC, or DSC) and whatever the value of alpha parameter (Table 3). As

Table 2. Thellier-Thellier archaeointensity results.

Sample	n	T_{min}	T_{max}	f	g	q	$DRAT$	H	F_{ATRM}	H_{ATRM}	F_{CR}	$H_{ATRM,CR}$
Kiln OSA												
OSA-1b	9	120	510	0.57	0.86	38.2	1.1	53.9 ± 0.7	0.988	53.2 ± 0.7	0.992	53.2 ± 0.7
OSA-1c	9	120	510	0.69	0.87	56.2	2.4	55.1 ± 0.6	0.992	54.7 ± 0.6	1.005	54.4 ± 0.6
OSA-2b	9	120	510	0.69	0.87	51.3	1.9	53.5 ± 0.6	0.946	50.7 ± 0.6	1.046	48.4 ± 0.6
OSA-2c	9	120	510	0.68	0.87	36.5	1.7	51.3 ± 0.8	0.991	50.9 ± 0.8	1.040	48.9 ± 0.8
OSA-3b	9	120	510	0.71	0.84	81.2	2.4	51.6 ± 0.4	0.985	50.9 ± 0.4	0.984	50.9 ± 0.4
OSA-3c	7	180	480	0.55	0.82	24.1	4.4	49.1 ± 0.9	0.995	48.9 ± 0.9	1.037	47.2 ± 0.9
OSA-4b	10	180	560	0.74	0.88	51.2	0.7	57.4 ± 0.7	0.974	55.9 ± 0.7	1.039	53.8 ± 0.7
OSA-4c	10	180	560	0.74	0.88	74.9	1.8	53.6 ± 0.5	1.006	53.9 ± 0.5	1.042	51.7 ± 0.4
OSA-5b	9	240	560	0.94	0.78	49.3	3.0	44.7 ± 0.7	1.052	47.0 ± 0.7	0.999	47.0 ± 0.7
OSA-5c	10	180	560	0.95	0.81	65.3	2.4	49.1 ± 0.6	0.981	48.2 ± 0.6	1.003	48.1 ± 0.6
OSA-6b	7	120	440	0.59	0.83	30.6	3.3	52.8 ± 0.9	0.989	52.2 ± 0.8	1.034	50.5 ± 0.8
OSA-6c	7	120	440	0.51	0.83	20.9	4.0	52.0 ± 1.1	1.003	52.1 ± 1.1	1.022	51.0 ± 1.0
OSA-7b	7	120	440	0.51	0.83	20.8	3.5	52.2 ± 1.1	0.986	51.5 ± 1.0	1.029	50.0 ± 1.0
OSA-7c	7	120	440	0.58	0.83	24.5	3.4	51.5 ± 1.0	1.006	51.7 ± 1.0	1.038	49.8 ± 1.0
OSA-7d	7	120	440	0.53	0.82	13.8	2.1	55.5 ± 1.7	0.992	55.1 ± 1.7	1.071	51.4 ± 1.6
OSA-9b	9	120	510	0.80	0.86	38.5	2.6	50.8 ± 0.9	0.966	49.1 ± 0.9	1.032	47.6 ± 0.9
OSA-9c	6	180	440	0.60	0.78	21.7	1.1	54.4 ± 1.2	1.002	54.5 ± 1.2	1.084	50.2 ± 1.1
OSA-10b	6	180	440	0.51	0.80	10.7	1.0	55.7 ± 2.1	1.010	56.3 ± 2.1	1.063	52.9 ± 2.0
OSA-10c	7	180	480	0.65	0.82	17.7	2.7	55.0 ± 1.7	1.021	56.1 ± 1.7	1.051	53.4 ± 1.6
OSA-11b	8	120	480	0.66	0.85	20.0	5.3	51.4 ± 1.4	1.019	52.3 ± 1.5	1.027	51.0 ± 1.4
OSA-11bii	8	120	480	0.69	0.85	19.5	2.6	49.0 ± 1.5	1.072	52.5 ± 1.6	1.034	50.7 ± 1.5
OSA-13b	9	120	510	0.70	0.87	25.8	2.5	49.2 ± 1.2	1.008	49.6 ± 1.2	1.019	48.6 ± 1.1
OSA-13c	10	120	540	0.78	0.89	37.8	1.9	49.8 ± 0.9	1.059	52.8 ± 1.0	1.017	51.9 ± 1.0
Unweighted Average								52.1 ± 2.9		52.2 ± 2.6		**50.6 ± 2.2**

To be continued

Table 2. Continuation.

Sample	n	T_{min}	T_{max}	f	g	q	$DRAT$	H	F_{ATRM}	H_{ATRM}	F_{CR}	$H_{ATRM,CR}$
Kiln OSB												
OSB-3cii	10	120	540	0.75	0.63	29.7	3.0	45.1 ± 0.7	1.012	45.6 ± 0.7	1.013	45.0 ± 0.7
OSB-4b	9	240	560	0.86	0.62	83.5	2.1	40.5 ± 0.3	1.000	40.5 ± 0.3	1.011	40.1 ± 0.3
OSB-4c	10	120	540	0.76	0.60	58.4	3.2	41.8 ± 0.3	0.990	41.4 ± 0.3	1.030	40.2 ± 0.3
OSB-4cii	10	120	540	0.75	0.61	65.5	3.3	45.4 ± 0.3	0.989	44.9 ± 0.3	1.033	43.5 ± 0.3
OSB-5b	10	120	540	0.74	0.88	19.5	2.2	62.9 ± 2.1	0.982	61.8 ± 2.1	1.004	61.6 ± 2.1
OSB-5c	8	120	480	0.73	0.85	22.4	2.8	60.7 ± 1.7	0.967	58.7 ± 1.6	1.025	57.3 ± 1.6
OSB-6b	10	120	540	0.77	0.88	45.2	3.0	47.3 ± 0.7	0.983	46.5 ± 0.7	1.007	46.2 ± 0.7
OSB-6c	7	20	400	0.59	0.83	20.1	4.6	45.2 ± 1.1	0.994	44.9 ± 1.1	1.032	43.5 ± 1.1
OSB-6d	9	120	510	0.70	0.87	33.7	1.9	46.7 ± 0.9	0.987	46.1 ± 0.8	1.010	45.6 ± 0.8
OSB-7b	9	120	510	0.50	0.81	22.0	2.3	53.3 ± 1.0	0.994	53.0 ± 1.0	1.035	51.2 ± 0.9
OSB-8aii	10	20	510	0.54	0.83	12.9	4.2	45.2 ± 1.6	0.989	44.7 ± 1.6	1.020	43.8 ± 1.5
Unweighted Average								48.6 ± 7.3		48.0 ± 6.9		**47.1 ± 6.9**

n is number of points in the interval of temperature T_{min}–T_{max} used to determine the archaeointensities. The fraction f of *NRM*, the gap factor g, and the quality factor q were calculated according to *Coe et al. (1978)*; *DRAT* corresponds to the difference ratio between repeat *pTRM* steps normalized by the length of the selected *NRM-pTRM* segment; H is the uncorrected archaeointensity estimate for individual specimen and uncertainty; F_{ATRM} and F_{CR} are the scaling factors for *TRM* anisotropy and cooling rate corrections, respectively; unweighted averages for uncorrected archaeointensities H, *ATRM*-corrected archaeointensities H_{ATRM}, and *ATRM* plus cooling rate corrected archaeointensities $H_{ATRM,CR}$.

recommended by *Fabian and Leonhardt (2010)*, if not significantly different from the others, the value obtained with the MSP-DSC ($\alpha = 0.5$) has to be chosen, that is 54.5 ± 3.5 μT for kiln OSA. The uncertainty is calculated from the regression analysis with the 95% confidence interval on the slope parameter estimate. This value is in good agreement and within the error bar with the value obtained with the conventional Thellier protocol.

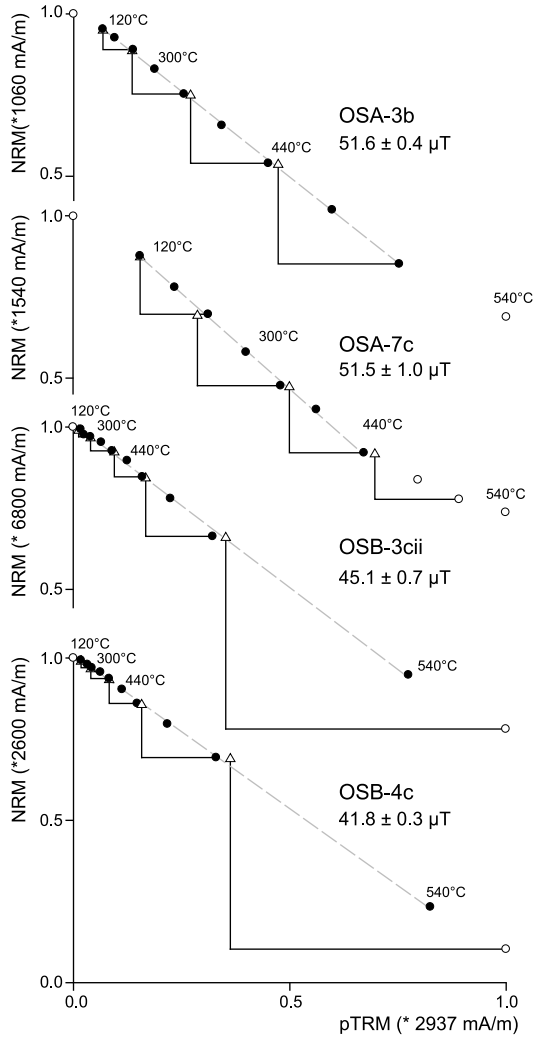

Fig. 9. Composite Arai diagrams for 2 samples from the kiln OSA and 2 samples from the kiln OSB, respectively. Solid (open) circles are *NRM-TRM* points accepted (rejected) to calculate the least squares line used to estimate the archaeointensity. Triangles denote the *pTRM* checks. *NRM* and *TRM* are normalized by the NRM_{max} and TRM_{max}, respectively.

Table 3. Multi-specimen protocol (MSP) results. Archaeointensity values (*PI*) are estimated by the zero-crossing point of the Robust linear regression on the *Q* parameters obtained with the MSP-DB protocol (*Dekkers and Bohnel, 2006*), fraction correction (MSP-FC) or domain state correction (MSP-DSC) protocols (*Fabian and Leonhardt, 2010*) as function of the laboratory field. The 95% confidence interval of the archaeointensity is calculated from the 95% confidence interval on the fitting line. R^2: coefficient of determination indicating how well data fit the model, *RMSE*: root mean squared error for the fitting line, *n*: number of data used to calculate the regression line; *N*: total number of data; α: parameter for the domain state correction (*Fabian and Leonhardt, 2010*).

Method	*PI* [μT]	95% conf.	*n*/*N*	R^2	*RMSE*
Kiln OSA					
MSP-DB	54.9	[51.1–59.4]	8/10	0.9739	0.0301
MSP-FC	54.3	[52.2–56.7]	8/10	0.9882	0.0450
MSP-DSC ($\alpha = 0.5$)	54.5	[51.6–57.8]	8/10	0.9584	0.3283
MSP-DSC ($\alpha = 0.2$)	54.6	[52.5–56.8]	8/10	0.9825	0.2435
MSP-DSC ($\alpha = 0.8$)	54.8	[51.0–59.0]	8/10	0.9234	0.3941
Preferred PI for OSA:	54.5 ± 3.5				
Kiln OSB					
MSP-DB	35.2	---	3/10	0.9747	0.0074
MSP-FC	55.7	[47.4–67.7]	3/10	0.6558	0.0884
MSP-DSC ($\alpha = 0.5$)	55.6	[47.8–66.3]	3/10	0.2559	0.3059
MSP-DSC ($\alpha = 0.2$)	56.0	[49.0–65.3]	3/10	0.5589	0.2968
MSP-DSC ($\alpha = 0.8$)	55.2	[46.6–67.6]	3/10	–0.2662	0.3179
Preferred PI for OSB:	Not reliable				

For kiln OSB, it has not been possible to calculate a MSP archaeointensity value. Seven out of the ten samples measured are rejected due to a too low *NRM* fraction. Evidently, the set temperature of 400°C that was a priori chosen to impart a significant *pTRM*, appeared to be too low for the majority of samples. This unsuccessful temperature choice is probably caused by the large heterogeneity in the magnetic properties that characterize the samples from OSB kiln. The remaining 3 accepted points are statistically poor: a best fitting line based on only 3 points would not be trustful.

5. ARCHAEOMAGNETIC DATING

The full geomagnetic field vector obtained for both OSA and OSB kilns has been used for archaeomagnetic dating after comparison with the reference SV curves calculated from the SCHA.DIF.3K regional geomagnetic field model (*Pavón-Carrasco et al., 2009*) at the site coordinates. Archaeointensity data obtained from the classical Thellier experiment, available for the two kilns have been used, even though the mean archaeointensity for OSB kiln is characterized by an important uncertainty (6.9 μT).

Possible ages at 95% confidence level have been calculated using the Matlab® archaeo-dating tool (*Pavón-Carrasco et al., 2011*). The final dating for each kiln is obtained after the combination of the separate density functions for declination,

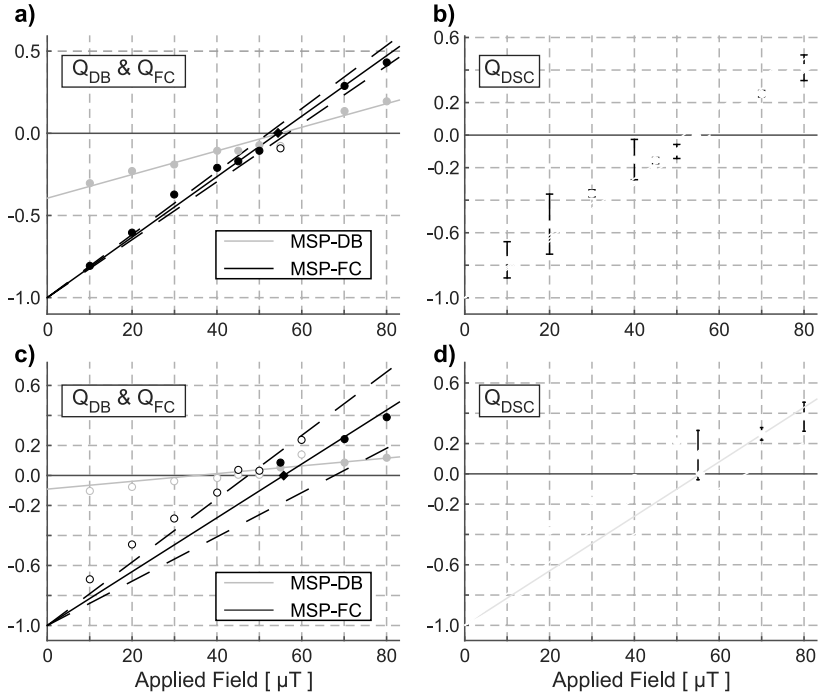

Fig. 10. Multi-specimen (MSP) archaeointensity determinations for **a)** and **b)** kiln OSA and **c)** and **d)** kiln OSB. Closed (open) symbols represent data used (rejected) in the robust regression of the responses in Q parameters on the predictors in magnetic field B. For MSP-DSC plots, data and fitting lines are calculated with $\alpha = 0.5$. The dashed lines are the 95% confidence intervals on the best fitting lines.

inclination and intensity. For OSA, archaeomagnetic dating suggests that the kiln has been for last time used in the time interval 1761–1841 A.D. (Fig. 11a). If we repeat the dating using the archaeointensity value obtained by the MSP technique (54.5 ± 3.5 μT) instead of that obtained by the Thellier experiment (50.6 ± 2.2 μT), the dating result remains practically the same (1760–1841 A.D.). For OSB kiln, archaeomagnetic dating based on the full geomagnetic field vector suggests that it has been abandoned between 1752 and 1831 A.D. (Fig. 11b). Exactly the same age is obtained if dating of the OSB kiln is repeated based only on directional results. These results clearly show that dating in the last few centuries A.D. is evidently controlled by the directions while archaeointensity results have almost no influence. The very small intensity variations of the Earth's magnetic field in Europe during the last five centuries (*Pavón-Carrasco et al., 2009*) result in the calculation of an associated too wide probability density (see intensity probability diagrams in Fig. 11) that makes dating resolution based on archaeointensity very low and therefore does not contribute to further constrain the dating results.

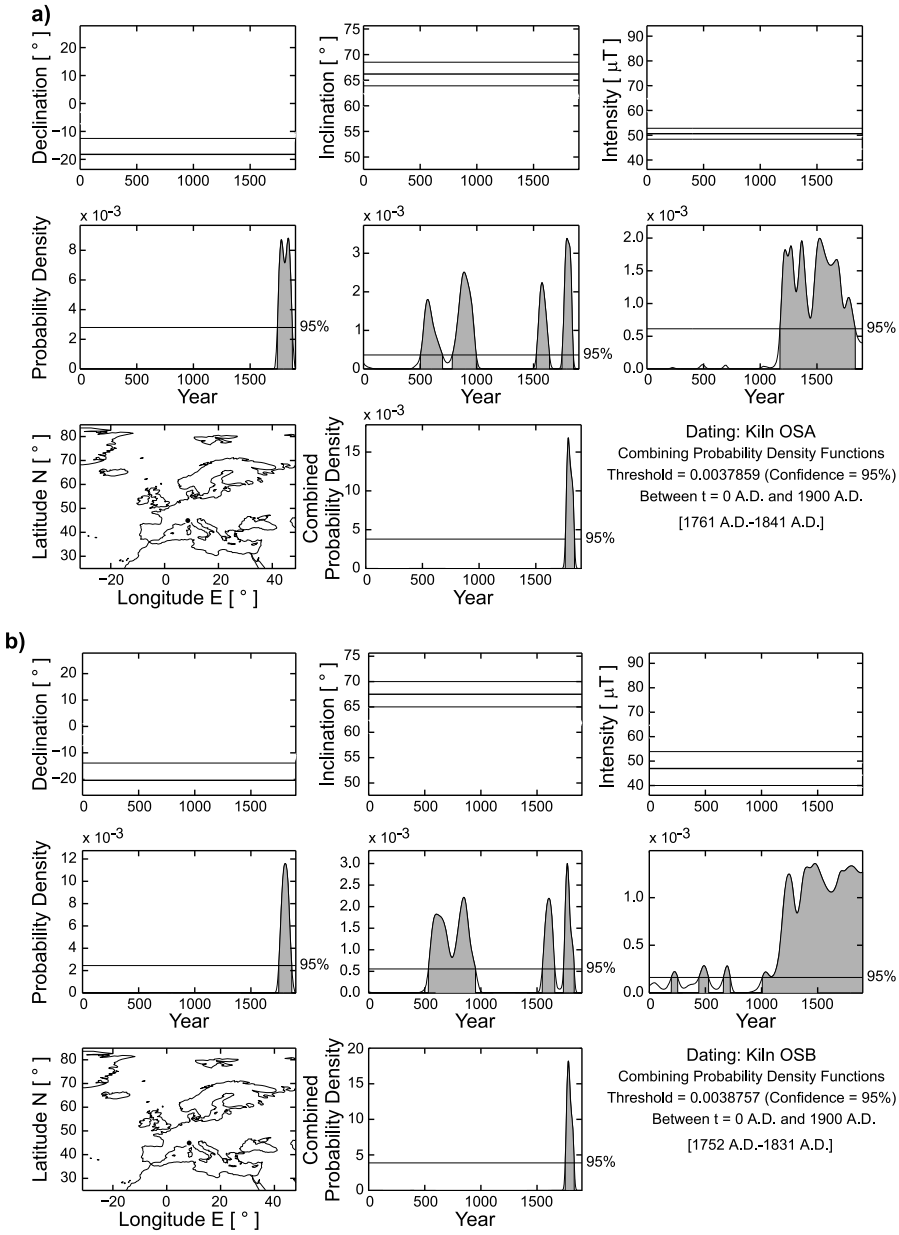

Fig. 11. Archaeomagnetic dating results for **a)** kiln OSA and **b)** kiln OSB. **Top:** declination (left), inclination (middle) and intensity (right) reference secular variation curves calculated from the SCHA.DIF.3K model (curve with error band) and the kiln's measured direction and intensity (straight line with error band); **middle:** calculated probability density functions for declination (left), inclination (middle) and intensity (right); **bottom:** location (left) and combined probability density function for declination, inclination and intensity (middle).

The dating results obtained here show that the two kilns were in use and abandoned almost contemporaneously, suggesting that they were constructed in order to satisfy the need of a large production of bricks. This dating is in good agreement with the archaeological findings of the site that suggest the presence of a big workshop at the area, with three big kilns already excavated. The hypothesis of the archaeologists that the bricks produced in the studied kilns could have been used for the construction of the fortification walls of the old city of Alessandria (Cittadella of Alessandria) is supported by our results. The Cittadella was designed by the Italian military architect Ignazio Bertola and was built between 1732 and 1808 A.D., with some last parts added as late as 1833 (e.g. Magazzino del Genio) (*Marotta, 1991*). Its construction undoubtedly needed a large quantity of bricks and the vicinity of the kilns to the fortified walls strongly supports such connection. However, other hypothesis suggesting that the produced bricks were used for the construction of the long bridge made by stones and bricks connecting to the Cittadella, and/or for the construction between 1749 and 1831 A.D. of several multi-storey buildings arranged along the axis of the ancient quarter of Bergoglio, are also in good agreement with our results and cannot be excluded.

6. CONCLUSIONS

Two big brick kilns excavated at Osterietta provided abundant material for a detailed rock-magnetic and archaeomagnetic study. Magnetic mineralogy analysis suggested the suitability of the material for both direction and intensity determinations, indicating the presence of thermally stable, mainly pseudo-single domain (PSD) magnetite as the main magnetic carrier. These results encouraged the use of both classical Thellier and the multi-specimen procedures for archaeointensity determination. The main results of our study can be summarized as follows:

1. Brick samples coming from the internal part of the kilns have been heated at high temperatures and have successfully registered the direction of the Earth's magnetic field at the time of their last cooling.
2. Both classical Thellier and multi-specimen (MSP) techniques have been successfully applied to OSA kiln, giving very similar results (statistically undistinguishable).
3. For kiln OSB, even though rock-magnetic analysis showed the presence of single-domain (SD) to PSD thermally stable magnetite grains, both Thellier and MSP methods have not given successful results. The archaeointensity determined by the classical Thellier method shows large standard deviation, about 13% of the average, probably due to important inhomogeneities between single bricks that result in discrepancies on the archaeointensity values determined at sample level. Using the MSP protocol, it was not possible to calculate a mean archaeointensity due to the very low natural remanent magnetization (*NRM*) fraction involved, probably caused by a not adequate temperature choice.
4. Archaeomagnetic dating suggests that the OSA kiln was last used between 1761–1841 A.D. and the OSB kiln between 1752–1831 A.D., at 95% probability. In the case of both kilns, dating based on the full geomagnetic field vector gave exactly the same results with dating based only on directions. This suggests, that

even when archaeointensities are well defined with small standard deviation (as in the case of kiln OSA), intensity results do not improve the precision of archaeomagnetic dating when referring to the last few centuries. That is because of the slight variations of the intensity of the Earth's magnetic field during the last five centuries.

5. The dating results obtained here support the hypothesis that the discovered kiln workshop was used for the production of bricks during the construction of the fortified walls of the Cittadella of Alessandria and/or the construction of secondary walls and buildings of the ancient quarter of Bergoglio that took place between 1749 and 1831 A.D.

SUPPLEMENTARY MATERIAL

Matlab® code estimating the factor *f* for *ATRM* correction during Thellier-Thellier experiment, v1.0 (01/01/2015), developed by Pierre CAMPS, CNRS and University of Montpellier, France (pcamps@univ-montp2.fr), can be downloaded from *http://ig.cas.cz/sites/default/files/Tema 2015-0013 supplementary.pdf*.

Acknowledgments: We would like to warmly acknowledge the "Soprintendenza per i Beni archeologici del Piemonte e del Museo Antichità Egizie" for sampling permission. Dr. Marica Venturino, Dr. Alberto Crosetto and ARKAIA s.r.l. are particularly acknowledged for providing useful information on the excavation and fruitful discussion on the use and dating of the kilns. We are grateful to Patrick Nicol for technical help during the laboratory experiments at the Montpellier laboratory. This project was part of the PHC-Galileo program. The Géosciences Montpellier was supported by a grant from the CNRS-PNP. The FUReMAG rapid furnace construction was supported by the French National Agency for Research (ANR-12-BS06-0015). The Editor Eduard Petrovský, the Associate Editor Mark Dekkers, and the reviewers Harald Böhnel and Angel Carrasco are warmly acknowledged for their useful comments on the manuscript.

References

Biggin A.J. and Poidras T., 2006. First-order symmetry of weak-field partial thermoremanence in multi-domain ferromagnetic grains. 1. Experimental evidence and physical implications. *Earth Planet. Sci. Lett.*, **245**, 438–453, DOI: 10.1016/j.epsl.2006.02.035.

Camps P., Singer B., Carvallo C., Goguitchaichvili A., Fanjat G. and Allen B., 2011. The Kamikatsura event and the Matuyama–Brunhes reversal recorded in lavas from Tjornes peninsula, northern Iceland. *Earth Planet. Sci. Lett.*, **310**, 33–44, DOI: 10.1016 /j.epsl.2011.07.026.

Casas L., Linford P. and Shaw J., 2007. Archaeomagnetic dating of Dogmersfield Park brick kiln (Southern England). *J. Archeol. Sci.*, **34**, 205–213.

Coe R.S., Grommé S. and Mankinen A., 1978. Geomagnetic paleointensities from radiocarbon-dated lava flows on Hawai and the question of the Pacific nondipole low. *J. Geophys. Res.*, **83**, 1740–1756.

Dekkers M. J. and Böhnel H.N., 2006. Reliable absolute palaeointensities independent of magnetic domain state. *Earth Planet. Sci. Lett.*, **248**, 508–517, DOI: 10.1016/j.epsl.2006.05.040.

De Marco E., Spassov S., Kondopoulou D., Zananiri I. and Gerofoka E., 2008. Archaeomagnetic study and dating of a Hellenistic site in Katerini (N. Greece). *Phys. Chem. Earth*, **33**, 481–495.

Dunlop D.J., and Ozdemir O., 2000. Effect of grain size and domain state on thermal demagnetization tails. *Geophys. Res. Lett*., **27**, 1311–1314.

Fabian K. and Leonhardt R., 2010. Multiple-specimen absolute paleointensity determination: an optimal protocol including pTRM normalization, domain-state correction, and alteration test. *Earth Planet. Sci. Lett.*, **20**7, 84–94.

Fanjat G., 2012. Les fluctuations du champ magnétique terrestre: des variations séculaires récentes aux renversements. Available online at https://tel.archives-ouvertes.fr/tel-00719380 (in French).

Fanjat G., Camps P., Alva-Valdivia L., Sougrati M., Cuevas-Garcia M. and Perrin M., 2013. First archaeointensity determinations on Maya incense burners from palenque temples, Mexico: new data to constrain the Mesoamerica secular variation curve. *Earth Planet. Sci. Lett.*, **363**, 168–180.

Fisher R.A., 1953. Dispersion on a sphere. *Proc. R. Soc. London A*, **217**, 295–305.

Gómez-Paccard M. and Beamud E., 2008. Recent achievements in archaeomagnetic dating in the Iberian Peninsula: application to Roman and Mediaeval Spanish structures. *J. Archeol. Sci.*, **35**, 1389–1398.

Herries A., Kovacheva M. and Kostadinova M., 2008. Mineral magnetism and archaeomagnetic dating of a mediaeval oven from Zlatna Livada, Bulgaria. *Phys. Chem. Earth*, **33**, 496–510.

Holland P.W. and Welsch R.E., 1977. Robust Regression using iteratively reweighted least-squares. *Commun. Stat.-Theory Methods*, **A6**, 813–827.

Jordanova N., Kovacheva M. and Kostadinova M., 2004. Archaeomagnetic investigation and dating of Neolithic archaeological site (Kovachevo) from Bulgaria. *Phys. Earth Planet. Int.*, **147**, 89–102.

Kirschvink J.L., 1980. The least-square line and plane and the analysis of palaeomagnetic data. *Geophys. J. R. Astron. Soc.*, **62**, 699–718.

Leonhardt R., Heunemann C. and Krása D., 2004. Analysing absolute paleointensity determinations: acceptance criteria and the software Thelliertool4.0. *Geochem. Geophys. Geosyst*., **5**, DOI: 10.1029/2004GC000807.

Lowrie W., 1990. Identification of ferromagnetic minerals in a rock by coercivity and unblocking temperature properties. *Geophys. Res. Lett.*, **17**, 159–162.

Marotta A., 1991. La cittadella di Alessandria: Una fortezza per il territorio dal Settecento all'Unità. SO.G.ED. Edizioni, Alessandria, pp. 170 (in Italian).

Pavón-Carrasco F.J., Osete M.L., Torta J.M. and Gaya-Piqué L.R., 2009. A regional archaeomagnetic model for Europe for the last 3000 years, SCHA.DIF.3K: applications to archaeomagnetic dating. *Geochem. Geophys. Geosyst.*, **10**, Q03013, DOI: 10.1029 /2008GC002244.

Pavón-Carrasco F.J., Rodriguez-Gonzalez J., Osete M.L. and Torta J., 2011. A Matlab tool for archaeomagnetic dating. *J. Archeol. Sci.*, **38**, 408–419.

Prévot M., Mankinen E.A., Coe R.S. and Grommé C., 1985. The Steens mountain (Oregon) geomagnetic polarity transition 2. Field intensity variations and discussion on reversal models. *J. Geophys. Res.*, **90**, 10417–10448.

Schnepp E. and Lanos P., 2006. A preliminary secular variation reference curve for archaeomagnetic dating in Austria. *Geophys. J. Int.*, **166**, 91–96.

Selkin P.A. and Tauxe L., 2000. Long-term variations in palaeointensity. *Philos. Trans. R. Soc. A-Math. Phys. Eng. Sci.*, **358**, 1065–1088.

Tema E. and Lanza R., 2008. Archeaomagnetic study of a lime kiln at Bazzano (Northern Italy). *Phys. Chem. Earth*, **33**, 534–543.

Tema E., 2013. Detailed archaeomagnetic study of a ceramic workshop at Kato Achaia: New directional data and archaeomagnetic dating in Greece. *Bull. Geol. Soc. Greece*, **XLVII**, No 3, 1279–1288.

Tema E., Fantino F., Ferrara E., Lo Giudice A., Morales J., Goguitchaichvili A., Camps P., Barello F. and Gulmini M., 2013. Combined archaeomagnetic and thermoluminescence study of a brick kiln excavated at Fontanetto Po (Vercelli, Northern Italy). *J. Archeol. Sci.*, **40**, 2025–2035.

Tema E., Fantino F., Ferrara E., Allegretti S., Lo Giudice A., Re A., Barello F., Vella S., Cirillo L. and Gulmini M., 2014. Archaeological, archaeomagnetic and thermoluminescence investigation of a baked clay kiln excavated at Chieri, northern Italy: contribution to the rescue of our cultural heritage. *Ann. Geophys.*, **57**, G0548, DOI: 10.4401/ag-6611.

Thellier E. and Thellier O., 1959. Sur l'intensité du champ magnétique terrestre dans le passé historique et géologique. *Ann. Geophys.*, **15**, 285–376 (in French).

Veitch R.J., Hedley I.G. and Wagner J.J., 1984. An investigation of the intensity of the geomagnetic field during Roman times using magnetically anisotropic bricks and tiles. *Archeol. Sci.*, **37**, 359–373.

Venturino Gambari M., Crosetto A. and Prosperi R., 2013. Alessandria, località Osterietta: Rinvenimento di fornaci postmedievali. *Quaderni della Soprintendenza Archeologica del Piemonte*, **28**, 187–189 (in Italian).

Zijderveld J., 1967. AC demagnetization of rocks: analysis of results. In: Collinson D., Creer K. and Runcorn S. (Eds), *Methods in Paleomagnetism*. Elsevier, New York, 254–256.